Scientific Research Publishing

Materials Sciences and Applications, 2024, 15, 417-430
https://www.scirp.org/journal/msa
ISSN Online: 2153-1188
ISSN Print: 2153-117X

Hydroxyapatite/Alginate Nanocomposite: *In Situ* Processing and Properties for Biomedical Applications

Suraya Sabrin Soshi[1], Syeda Kariumnnesa[2*], Mohammad Abdul Gafur[3*]

[1]Department of Mechanical and Production Engineering, Ahsanullah University of Science and Technology, Dhaka, Bangladesh
[2]Department of Physics, University of Chittagong, Chittagong, Bangladesh
[3]Bangladesh Council of Scientific and Industrial Research, Dhaka, Bangladesh
Email: *karimunnesa@cu.ac.bd, *d_r_magafur@yahoo.com

How to cite this paper: Soshi, S.S., Kariumnnesa, S. and Gafur, M.A. (2024) Hydroxyapatite/Alginate Nanocomposite: *In Situ* Processing and Properties for Biomedical Applications. *Materials Sciences and Applications*, **15**, 417-430.
https://doi.org/10.4236/msa.2024.1510028

Received: August 22, 2024
Accepted: October 9, 2024
Published: October 12, 2024

Abstract

The development of advanced biomaterials is crucial for addressing the increasing demand for improved medical implants and tissue engineering scaffolds. Hydroxyapatite (HAp), a naturally occurring mineral form of calcium apatite, is widely recognized for its excellent biocompatibility and osteoconductivity, making it an ideal candidate for bone-related applications. However, its brittleness and lack of flexibility limit its broader application in dynamic biological environments. To overcome these limitations, this study explores the synthesis of Hydroxyapatite/Alginate (HAp/Alg) nanocomposites, leveraging the biocompatibility and flexibility of alginate—a natural polysaccharide derived from brown seaweed. The HAp/Alg nanocomposites were synthesized using *in situ* hybridization techniques with varying alginate concentrations (10 to 40 wt%) to optimize their structural and functional properties. The motivation behind this work lies in the potential of these composites to combine the desirable properties of both HAp and alginate, resulting in a material that not only mimics the mineral composition of bone but also offers enhanced flexibility and structural integrity. A comprehensive analysis was conducted using X-ray Diffraction (XRD), Fourier Transform Infrared Spectroscopy (FT-IR), Thermogravimetric Analysis/Differential Thermal Analysis (TGA/DTA), Scanning Electron Microscopy (SEM), and cytotoxicity testing to evaluate the structural, chemical, and biological properties of the composites. XRD analysis indicated a complex interaction between alginate concentration and crystal growth, with crystallite size increasing up to 10 wt% alginate before decreasing. FT-IR spectra confirmed significant biological reactivity at the composite's surface and within the polymer matrix, suggesting strong potential for biological interactions. SEM images revealed a more uniform

microstructure in HAp/Alg composites compared to pure HAp, which is likely to improve their performance in biomedical applications. TGA/DTA results demonstrated the thermal stability of the composites across various temperature conditions, while cytotoxicity tests confirmed their biocompatibility, making them suitable for use in medical applications. This study not only successfully synthesizes HAp/Alg nanocomposites with enhanced structural uniformity and biocompatibility but also provides a promising avenue for the development of next-generation biomaterials that could significantly impact the field of regenerative medicine and biomedical engineering.

Keywords

HAP, TG/DTA, XRD

1. Introduction

Native bone tissue possesses a nanocomposite structure, mainly composed of non-stoichiometric Hydroxyapatite (HAp; $Ca_{10}(PO_4)_6(OH)_2$) and collagen fiber matrix, that provide appropriate physical and biological properties, especially mechanical support and protection from the vertebrate skeleton. However, bone needs to be repaired or regenerated upon damage. In the USA, there are estimated 280,000 hip fractures, 700,000 vertebral and 250,000 wrist fractures each year. The demand in the surgical market is underscored by the fact that around 4 million bone grafting or bone substitute procedures are conducted worldwide each year [1]. Currently, different types of bone grafts and bone graft substitutes, such as autografts, allografts and alloplastic or synthetic bone grafts, are used for surgical treatments [2] [3]. Autografts compose approximately 58% of the bone substitutes, whereas allografts constitute approximately 34% [2]. As autografts have all the properties necessary for new bone growth, they are considered the gold standard for bone repair. However, the disadvantages of autografts include limited availability, donor site morbidity and risk of disease transmission from donor to recipient [3] [4]. Therefore, allografts are attractive alternatives to autografts; however, they are not usually osteoinductive or osteogenic, they have risks of an immunological reaction or disease transmission and they have insufficient mechanical properties for load bearing bone applications. Therefore, there is a great demand for synthetic grafts for fracture repair, and there is also scope to improve existing graft materials. Therefore, it gives rise to an abundant demand for safe and effective materials for use in bone tissue regeneration [5]-[7].

The specific requirements for the ideal materials are good mechanical properties, biocompatibility and controlled resorbability. Good mechanical properties mean that the materials (including biodegradable and bioresorbable materials) are able to maintain their structural integrity and stability. Biocompatibility provides the material with the ability to be compatible with living tissue or a living system without causing harm. Various materials of biological and synthetic origin have

been used for bone tissue regeneration [8].

However, most commercially available and FDA-approved orthopedic implants rely on a limited selection of biomaterials, whose mechanical properties often differ significantly from those of the extracellular matrix (ECM) of bone. Common materials include stainless steel, cobalt-chrome, and titanium alloys. Ceramics include alumina, zirconia, HAp, and other calcium phosphates. Polymers include chitosan, gelatine, alginate, ultra-high molecular weight polyethylene (UHMWPE), polymethyl methacrylate (PMMA), and polyaryletherketone (PAEK) [9]. Most metals and ceramics are much stiffer than bone tissue, which can result in mechanical mismatch ("stress shielding") between the implant and the adjacent bone tissue, including a loss of integrity at the bone/implant interface due to resorption of bone tissue [10]. On the other hand, most polymers are more compliant than bone tissue and unable to bear physiological levels of load [11]. In recent years, the search for innovative bone substitutes to develop this new therapeutic concept has gradually moved to non-metallic composite materials because they can closely mimic the hierarchical and nanoscale composite structure of native bone [6] [12].

Nanocomposites made of biocompatible polymers and bioactive inorganic nanoparticles have attracted particular attention for use as bone tissue regeneration materials and even permanent bone substitutes due to their excellent mechanical properties and biocompatibility [13] [14]. A bioactive material is a material that creates a specific biological response at the interface of the material to help bond formation between the material and the tissues. Therefore, a bioactive material can help to generate a series of biophysical and biochemical reactions at the implant-tissue interface when it is implanted in the body [13]. In comparison with the single-component materials, the new generation of materials can synergistically combine the advantages of polymers (e.g., low weight, biocompatibility, desired shape and resistance to corrosion) with the bioactive properties of inorganic nanoparticles. The bioactivity of these nanocomposites originates from the bioactive inorganic nanoparticles, such as native or synthetic HA, tricalcium phosphate (TCP), calcium carbonate, bioactive glass and glass ceramic, known as apatite-wollastonite [2] [15]. Their biocompatibility is considered to arise from their chemical structural similarity to the components of the native bone. On the other hand, the excellent mechanical properties and moldability are provided by the polymers, most of which are biocompatible, such as gelatin, alginate, collagen, chitosan, bacterial cellulose PLA, polyurethane, ultrahigh-molecular weight polyethylene (UHMWPE), poly (etherketone) and polycaprolactone, etc [8].

Research on bioceramics (ceramics, carbon, glass and glass-ceramics) has attracted considerable attention because of their potential for biocompatibility and bioactivity with the human body. Considerable research has been reported in the development of calcium phosphate ceramics as implants [9]. In recent years, nanohydroxyapatite (n-HAp) powders have been crucial in biomedical applications because of its similarity with the bone mineral. An increase in the surface area of n-

HAp leads to a greater proportion of its atoms or molecules being displayed on its surface rather than in the interior. As a result, it enhances biological performance, such as cell adhesion, osteointegration, proliferation and differentiation, which, in turn, facilitates the growth of new bone tissue within a short period of time. The biomedical applications of n-HAp have been studied extensively [16]. Nonetheless, hydroxyapatite, nano-crystal, makes it difficult to form specific formula needed for bone repair and implantation. This is due to the intrinsic hardness, fragility, and lack of flexibility, thereby restricting the use of it as a load-bearing implant material [17].

There is always a problem encountered with HAp-based implants, which are that HA particles easily migrate from the implanted sites into surrounding tissue when mixed with patient's body fluid and blood. The migration causes damage to healthy tissue and thus, therapeutic efficiency is not satisfactory. Bearing this in mind, the complete fusion of hydroxyapatite nanoparticles in the alginate matrix is beneficial for particulate immobilization [18]-[20]. Besides this, the inclusion of nanoparticles of hydroxyapatite into the biocompatible alginate matrix mitigates the inherent brittleness and moldability while giving nanotopographic features that mimic the nanostructure of bone and shows good osteoconductivity to bridge the gap between implants and cortical bone without any adverse reaction [12] [18].

Hydroxyapatite/Alginate (HAp/Alg) nanocomposites have been prepared using a number of methods such as phase separation, droplet extrusion, dispersion polymerization, biomimetic mineralization, self-assembling techniques [18] [21]-[25] co-precipitation [26] freeze extrusion [27], etc. Recently, material researchers have exploited *in situ* hybridization aimed at producing chemically and biologically improved HAp/polymer composites as bone substitute materials. The advantage of this method over mechanical mixing is that the binding strength at the inorganic-organic interface can be enhanced by the established chemical interaction between HA and the polymer matrix.

Although HA's chemical similarity to bone makes it an excellent candidate for bone grafting, its brittleness, inadequate mechanical properties, and tendency to migrate from the implant site into surrounding tissues limit its use as an implant material. Incorporating HA into an alginate matrix enhances its osteoconductivity and mechanical properties while also preventing the migration of HA particles into surrounding tissues. However, several studies have highlighted that conventional mechanical mixing of HAp granules with Ca^{2+}-crosslinked alginate to create HA-alginate nanocomposites often leads to poor physicochemical homogeneity and insufficient interfacial bonding between the mineral and polymer phases. The objective of this study was to synthesize an HAp/Alg nanocomposite with improved chemical and structural homogeneity, as well as to gain deeper insights into its microstructure and physicochemical properties.

While a variety of materials and methods have been employed for bone regeneration, the development of bioactive inorganic nanoparticle-polymer nanocomposites

has shown significant promise due to their biocompatibility and mechanical properties. Previous research has explored the use of materials such as hydroxyapatite (HAp), zirconium dioxide, and other polymers, but these efforts often face challenges related to mechanical mismatch and stress shielding between implants and bone, as well as limitations in the load-bearing capacity of the materials.

The incorporation of hydroxyapatite nanoparticles into biocompatible matrices like alginate has been particularly noteworthy. This combination enhances moldability, reduces brittleness, and better mimics the nanostructure of bone, which is crucial for effective bone regeneration. While *in-situ* hybridization techniques have advanced the development of these HAp/polymer composites, the method itself does not represent a significant departure from existing techniques.

This study builds upon the foundational work by optimizing the crystalline structure and physical properties of HAp/Alg nanocomposites. Unlike earlier efforts that primarily focused on the mechanical integration of materials, this research emphasizes achieving chemical and structural consistency within the composite, which is critical for enhancing its performance as a bone substitute. The *in-situ* hybridization method, while advantageous, is leveraged here not as a novel technique but as a means to achieve superior material properties that could overcome the limitations identified in previous studies.

2. Experimental Details

Hydroxyapatite (HAp) and Hydroxyapatite/Alginate (HAp/Alg) nanocomposites, with alginate amounts varying from 10 to 40 wt%, were synthesized by *in-situ* hybridization method using $Ca(OH)_2$, H_3PO_4, Na-alginate and $CaCl_2$ as precursor materials.

An alginate gel solution (2% w/v) was prepared by dissolving alginate powder into de-ionized water (DIW). Next, a 100 ml solution of 1M $Ca(OH)_2$ (7.40 g/100 ml, 97% purity) and a 0.6 M solution of ortho-H_3PO_4 (3.44 ml/100 ml, 85% purity) were prepared in separate beakers. The alginate gel solutions were then added dropwise to the $Ca(OH)_2$ solution while being vigorously agitated, and the mixture was stirred for an additional 30 minutes. Then, the solution of orthophosphoric acid was added in drops into the alginate/$Ca(OH)_2$ suspension. The solution was continuously stirred during H_3PO_4 addition period. The pH was kept above 10.5 throughout the reaction by the addition of ammonium hydroxide (NH_4OH) (25%) solution. The reaction temperature was maintained at 25˚C, and the mixture was stirred overnight. The next day, a 10 ml solution of $CaCl_2$ (0.1 mol/L) was added slowly to provide Ca^{2+} ions for crosslinking the alginate. After 30 minutes of crosslinking, the gel-like mixture was centrifuged at 5000 rpm for 30 minutes, followed by three washes with water to purify the precipitate. The precipitate was then vacuum-dried at 60˚C overnight and subsequently ground into a fine powder using an agate mortar. Meanwhile, pure HAp without alginate was prepared as a control sample using the same procedure.

The synthesized HAp/Alg nanocomposites, and pure Hydroxyapatite (HAp) were characterized both analytically and biologically. X-ray diffraction (XRD) analysis was conducted using a Bruker AXS diffractometer to determine the crystalline phase composition of the prepared powder, employing Kα radiation generated at 40 kV over a range of 20˚ to 80˚ (2θ). Crystallite size was also measured by XRD. The chemical compositions of synthesized nanocomposites, pure HAp, and pure alginate were confirmed by FT-IR (model: Brukers). Thermo-Gravimetric Analysis (TGA) of pure HAp and nanocomposite can be done in Thermo-Gravimetric Analyzer (EXSTAR 6000 TG/DTA 6300, Seiko Instruments Inc, Japan). TGA was used to determine the thermal stability of pure HAp and prepared composites with the gradual increase of temperature. To study the surface morphology and microstructure, a scanning electron microscope (SEM; JSM 7600F, JEOL-Japan) was used to observe the surface of the samples. Cytotoxicity was assessed using an inverted light microscope (Olympus, Japan) after 24 and 48 hours of incubation, with duplicate wells for each sample. The tests were conducted using human cervical carcinoma HeLa cells.

3. Result and Discussion

3.1. Crystalline Phase Composition and Size by XRD

The superimposed XRD pattern of the HAp/Alg composites: HAp90/alginate, HAp80/Alg, HAp70/Alg and HAp60/Alg and pure HAp are shown. Diffraction peaks of (211), (300) and (202) can be discerned as three individual peaks in pure HAp. XRD pattern of pure alginate exhibits a typical amorphous substance diffraction. When alginate is added in HAp, the characteristic peaks appear broadened and corresponding to those of HAp with a very low degree of crystallinity.

Additionally, the overlapping of the diffraction peaks is present in all samples, particularly in HAp/Alg composites. It indicates that the precipitated HAp crystals have small size and low crystallinity similar to natural bone mineral [19]. The poor crystalline nature of the as prepared HAp is possibly attributed to the wet-chemical synthesis at room temperature and the subsequent low temperature drying rather than sintering. From HAp to HAp60/Alg, the peak intensity decreases and the peak tends to be broader, *i.e.*, the full width at half maximum (FWHM) of the (002) peak shows an apparent increase. This can be taken as a sign for the decreased crystallinity of HAp with an increase in alginate content. The findings demonstrate that the presence of alginate affects the HAp crystal growth and therefore the crystallographic characteristics of HAp.

The crystallite size can be quantitatively evaluated from the XRD data using the Debye-Scherrer equation, which gives a relationship between peak broadening in XRD and particle size. $D = k\lambda/\beta\cos\theta$, where k is Scherrer constant (0.89), λ is the X-ray wavelength (nm), β is the fullwidth of half-maximum, and θ is the Bragg diffraction angel. **Table 1** shows the crystallite size of pure HAp and HAp/Alg composites.

Table 1. Crystallite size of pure HAp and HAp/Alg composites.

Sample	Crystallite size (nm)
HAp	12.19
HAp90/Alg	13.85
HAp80/Alg	12.15
HAp70/Alg	11.91
HAp60/Alg	7.74

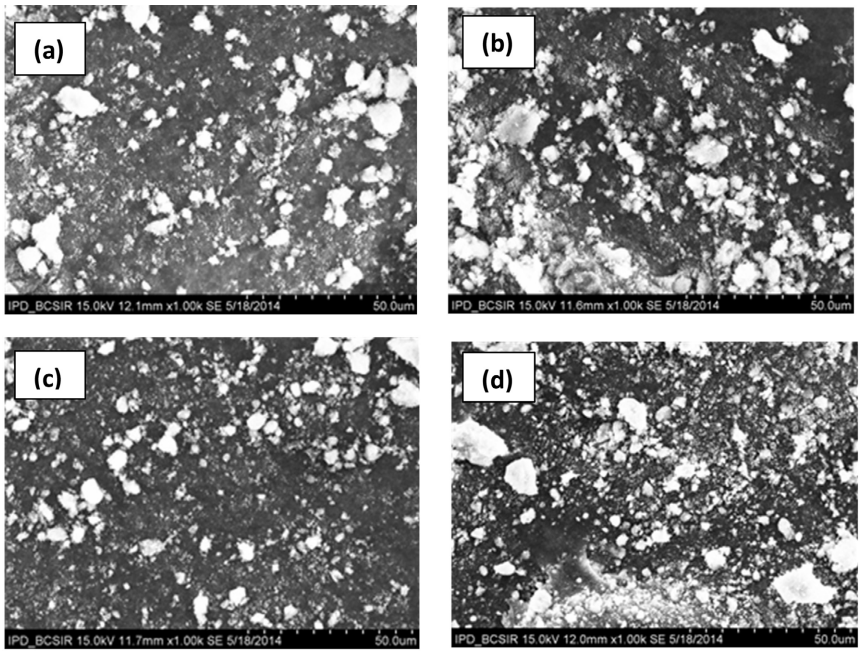

Figure 1. SEM image of pure HAp (a) and HAp/Alg composites: HAp90/alginate (b), HAp70/Alg (c) and HAp60/Alg (d).

3.2. Chemicalstate Analysis by FT-IR Spectra

3.2.1. SEM Analysis

Size and morphology of synthesized pure HAp and HAp/Alg composites: HAp90/alginate, HAp70/Alg and HAp60/Alg were observed by SEM in **Figure 1**.

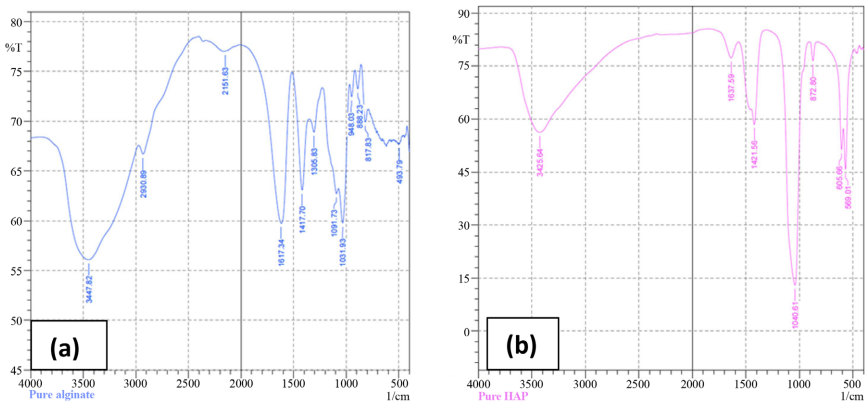

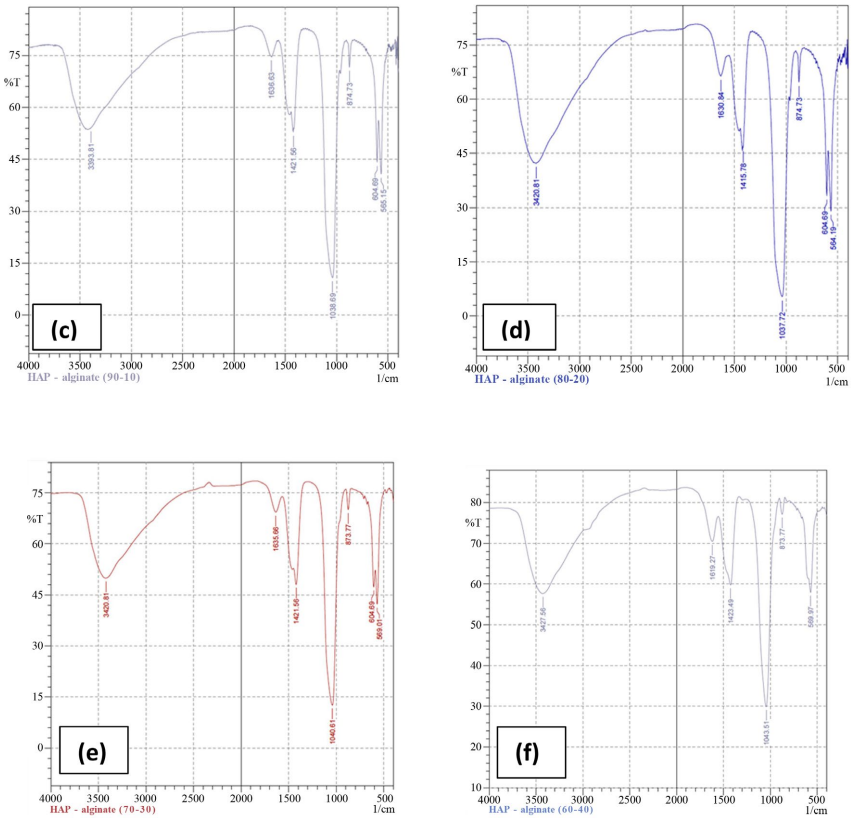

Figure 2. FT-IR spectra of pure alginate before cross linkage (a), pure HAp (b), HAp/Alg composites; HAp90/Alg (c), HAp80/Alg (d), HAp70/Alg (e) and HAp60/Alg (f).

Obtained image showed that pure HAp exhibits a loose discrete and in homogeneous microstructure. Weak electrostatic attractive forces loosely bind the particles to each other**.** In HAp/Alg composes the interfacial boundary between mineral and organic phases decreases with the increase of alginate contents leading to more homogeneous microstructure compared to pure HAp. The average particle size of pure HAp, HAp90/Alg, HAp70/Alg and HAp60/Alg is 200 - 300 nm, 400 nm, 500 nm and 800 nm - 1 μm respectively.

FT-IR spectra of Alginate before cross linkage in **Figure 2(a)**, pure HAp (b), HAp/Alg composites; HAp90/Alg (c), HAp80/Alg (d), HAp70/Alg (e) and HAp60/Alg (f) are given below.

The Fourier Transform Infrared (FTIR) spectra of the sodium alginate in **Figure 2(a)**, showed important absorption bands regarding hydroxyl, ether and carboxylic functional groups. Stretching vibrations of O-H bonds of alginate appeared at around 3448 $cm^{-1}$and that of aliphatic C-H was at around 2930.89 cm^{-1} [28]. Observed bands in 1617.34 $cm^{-1}$and 1417.70 cm^{-1} were attributed to asymmetric and symmetric stretching vibrations of carboxylate ion (COO^{-}) in alginate respectively. Later bands are very significant and can be used for characterization of alginate structure from its derivatives and ingredients. The bands at 1091 cm^{-1}were attributed to the C-O stretching vibration of ether functional groups [18]. In **Figure 2(b)**, pure HAp the bands at 1040 cm^{-1}, 605.66 cm^{-1} and 569.01

cm^{-1} corresponds to different vibrational modes of PO_4 groups in alginate. The bands at 1421.56 cm^{-1} and 872.80 cm^{-1} are derived from carbonate ion $\left(CO_3^2\right)^-$. No carbonate source was introduced into the starting materials and all the samples were prepared in an atmospheric environment. The incorporation of carbonate ion in HAp may be due to CO_2 gas present in environment. These typical bands from HAp have also been witnessed in the composites. The band at 1637.59 cm^{-1} is attributed to H_2O group in HAp. This band appears separately as a sharper band at 1619 cm^{-1} to 1636 cm^{-1} in the composites with different amount of alginates (**Figure 2(c)-(f)**), possibly due to the overlap of H_2O group of HAp and COO^- (at 1617 cm^{-1}) of alginate. From alginate to the composites, there are notable band shifts towards higher wave numbers found in the asymmetric stretching mode of COO^-; *i.e.*, a blue shift of 18 cm^{-1} from alginate to HAp70/Alg. The blue shifts imply that there exists chemical interaction between the mineral phase and organic materials due to chemical bonding between Ca^{2+} and negative charged carboxyl group in alginate [18] [29].

3.2.2. Thermo Gravimetric Analysis

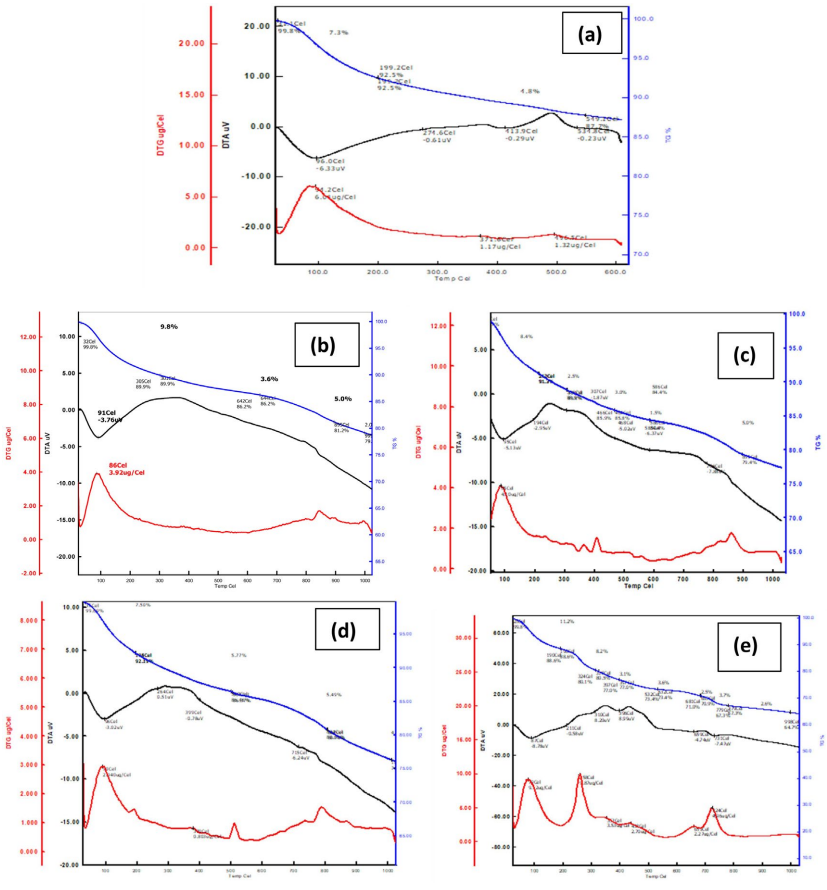

Figure 3. TGA, DTG, and DTA curve of pure HAp (a), HAp/Alg composites: HAp90/Alg (b), HAp80/Alg (c), HAp70/Alg (d) and HAp60/Alg (e).

The thermal behavior of the particles were studied using thermo-gravimetric

analysis (TGA) and the characteristic parameters of degradation of the tested samples were observed from thermo-gravimetry (TG) and first-order derivative (DTG) curves. Thermo-gravimetric analysis was carried out using TGA/6300 from 0˚C to 600˚C for pure HAp and from 0˚C to 1000˚C for HAp/Alg composites at a heating rate of 20˚C/minute under a nitrogen atmosphere. This analytical technique used to determine material's thermal stability and its fraction of volatile components by monitoring the weight loss of the sample in a chosen atmosphere as a function of temperature. TG, DTG, and DTA curve of pure HAp **Figure 3(a)**, HAp/Alg composites; HAp90/Alg **Figure 3(b)**, HAp80/Alg **Figure 3(c)**, HAp70/Alg **Figure 3(d)** and HAp60/Alg **Figure 3(e)** are given above.

In **Figure 3(a)**, TGA and DTGA of pure HAp shows that it exhibited two distinct weight loss stages at 31.1˚C - 199.2˚C (7.3%) and 199.2˚C - 549.1˚C (4.8%). 1st one is due to loss of adsorbed water without any effect on lattice parameter. And 2nd one is due to loss of lattice water caused by contraction in the *a*-lattice dimension during heating. The total weight loss of pure HAp is 12.3%. First order derivative of TGA curves revels the temperature at which the maximum decrease of mass occur. The temperature at the maximum loss rate is 92.2˚C [30].

The TGA and DTGA of HAp/Alg composites: HAp90/Alg, HAp80/Alg and HAp70/Alg (**Figure 3(b)-Figure 3(d)**) show that all of them exhibited two distinct weight loss stages. 1st one at 110 - 300˚C (maximum 9.8% and minimum 7.5%) and 2nd one at 600˚C - 900˚C (maximum 5.49% and minimum 5%). 1st weight loss is due to the decomposition of oligosaccharide and second weight loss is due to decomposition of polysaccharides [31]. In all the samples weight loss below 100˚C is due to evaporation of water. The total weight loss of HAp90/Alg, HAp80/Alg and HAp70/Alg is 20.4%, 20.6%, and 22.76% respectively. First order derivative of TGA curves revels the temperature at which the maximum decrease of mass occur. The temperatures at the maximum loss rate are 86˚C, 85˚C and 90˚C respectively.

The TGA and DTGA HA60/Alg composite in **Figure 3(e)** shows a different profile characterized by broad transitions. Maximum weight loss occurs at two stages. 1st at 100˚C - 190˚C (11.2%) and 2nd at 200˚C - 325˚C (8.2%). From 325˚C - 900˚C weight losses gradually and reaches to a final weight loss of about 35.3%. In all the samples weight loss below 100˚C is due to evaporation of water. First order derivative of TGA curves revels the temperature at which the maximum decrease of mass occur. The temperature at the maximum loss rate is 258˚C.

3.2.3. Cytotoxicity Analysis

The purpose of the investigation was to evaluate potential cytotoxicity to show the effects of HAp and HAp/Alginate composite on the viability of cells growth in culture. The HeLa cells were exposed to pure HAp and HAp/Alg composite with a concentration of 50 μg/ml for 24 and 48 hours. Dimethyl Sulfoxide (DMSO) and De-ionized water (DIW) was used as a positive control media and HeLa cell was used as negative control media. **Figure 4** (left side) showed clear images of cellviability for

control media, pure Hap and HAp70/Alginate respectively after 24 and 48 hours of incubation. The cell viability was 100% in the control media and more than 95% in both HAp and HAp70/Alg composites. This result indicated that HAp and HAp/Alg composite have no cytotoxicity on HeLa cell.

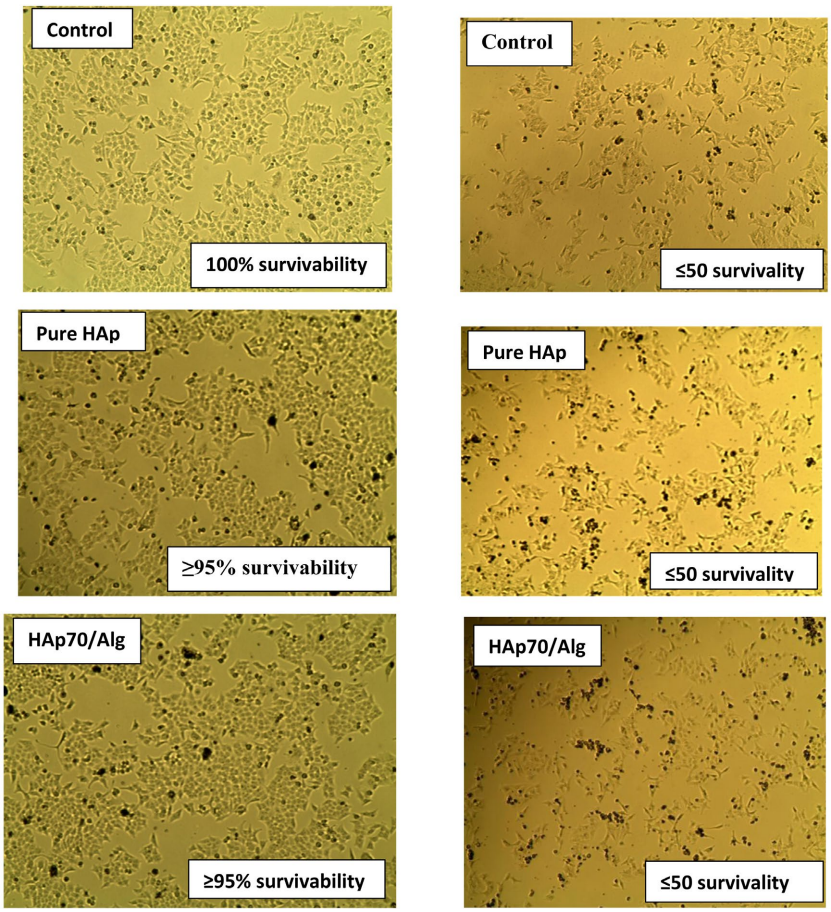

Figure 4. Cytotoxycity effect of DIW on control media, pure HAp and HAp70/Alg on HeLa cell (left site) and DMSO on control media, pure HAp and HAp70/Alg on HeLa cell (right site).

Figure 4 shows clear images of cellviability for control media, pure HAp and HAp70/Alginate respectively after 24 and 48 hours of incubation (right side). The HeLa cells were exposed to DMSO for 24 and 48 hours and showed a clear image of cell death of about 50% for DMSO. This result demonstrated that DMSO has cytotoxic effect on carcinoma cell lines. Additionally, cell death for pure HAp and HAp70/Alg composite was also about 50%. From the observation of the below figures we can conclude that cell death was due to DMSO and pure HAp and HAp70/Alg nanocomposite was not responsible for cell death.

4. Conclusions

This study successfully synthesized HAp/Alg nanocomposites with varying weight ratios through *in situ* hybridization, providing a comprehensive characterization

using SEM, XRD, FT-IR, TGA, and cytotoxicity tests. The results demonstrated that the incorporation of alginate into hydroxyapatite significantly alters the crystallographic structure, leading to a weakly crystalline HAp that closely resembles biological apatite. This alteration is confirmed by FT-IR analysis, which revealed a strong interaction between the calcium ions in HAp and the carboxyl groups in alginate.

Morphological analysis indicated that the addition of alginate results in a finer microstructure compared to pure HAp, which may have implications for the material's functionality in biomedical applications. Moreover, the biocompatibility of the synthesized nanocomposites was confirmed by cytotoxicity studies, suggesting that these materials are suitable for potential use in medical devices or tissue engineering.

Despite the promising findings, the study acknowledges that further research is needed to fully optimize the properties of HAp/Alg nanocomposites. Future work should explore ways to enhance their mechanical properties and investigate their long-term stability and performance in biological environments. This will be crucial for advancing the application of these nanocomposites in clinical settings, where mechanical strength and durability are essential.

In conclusion, while this study contributes valuable insights into the synthesis and characterization of HAp/Alg nanocomposites, ongoing research is necessary to address the remaining challenges and fully realize their potential in biomedical applications.

Acknowledgements

The authors duly acknowledge the authority of Bangladesh Council of Scientific and industrial Research (BCSIR).

Conflicts of Interest

There is no conflict of interest to declare.

References

[1] Brydone, A.S., Meek, D. and Maclaine, S. (2010) Bone Grafting, Orthopaedic Biomaterials, and the Clinical Need for Bone Engineering. *Proceedings of the Institution of Mechanical Engineers, Part H: Journal of Engineering in Medicine*, **224**, 1329-1343. https://doi.org/10.1243/09544119jeim770

[2] James, R., Deng, M., Laurencin, C.T. and Kumbar, S.G. (2011) Nanocomposites and Bone Regeneration. *Frontiers of Materials Science*, **5**, 342-357. https://doi.org/10.1007/s11706-011-0151-3

[3] Duan, B., Wang, M., Zhou, W.Y., Cheung, W.L., Li, Z.Y. and Lu, W.W. (2010) Three-dimensional Nanocomposite Scaffolds Fabricated via Selective Laser Sintering for Bone Tissue Engineering. *Acta Biomaterialia*, **6**, 4495-4505. https://doi.org/10.1016/j.actbio.2010.06.024

[4] Goulet, J.A., Senunas, L.E., DeSilva, G.L. and Greenfield, M.L.V.H. (1997) Autogenous Iliac Crest Bone Graft: Complications and Functional Assessment. *Clinical Orthopaedics*

and Related Research, **339**, 76-81.
https://doi.org/10.1097/00003086-199706000-00011

[5] Wagoner Johnson, A.J. and Herschler, B.A. (2011) A Review of the Mechanical Behavior of Cap and Cap/Polymer Composites for Applications in Bone Replacement and Repair. *Acta Biomaterialia*, **7**, 16-30. https://doi.org/10.1016/j.actbio.2010.07.012

[6] Scholz, M., Blanchfield, J.P., Bloom, L.D., Coburn, B.H., Elkington, M., Fuller, J.D., *et al*. (2011) The Use of Composite Materials in Modern Orthopaedic Medicine and Prosthetic Devices: A Review. *Composites Science and Technology*, **71**, 1791-1803. https://doi.org/10.1016/j.compscitech.2011.08.017

[7] Yu, N.Y.C., Schindeler, A., Little, D.G. and Ruys, A.J. (2010) Biodegradable Poly(*α*-Hydroxy Acid) Polymer Scaffolds for Bone Tissue Engineering. *Journal of Biomedical Materials Research Part B*: *Applied Biomaterials*, **93**, 285-295. https://doi.org/10.1002/jbm.b.31588

[8] Sahoo, N.G., Pan, Y.Z., Li, L. and He, C.B. (2013) Nanocomposites for Bone Tissue Regeneration. *Nanomedicine*, **8**, 639-653. https://doi.org/10.2217/nnm.13.44

[9] Roeder, R.K., Converse, G.L., Kane, R.J. and Yue, W. (2008) Hydroxyapatite-Reinforced Polymer Biocomposites for Synthetic Bone Substitutes. *JOM*, **60**, 38-45. https://doi.org/10.1007/s11837-008-0030-2

[10] Bobyn, J.D., Mortimer, E.S., Glassman, A.H., Engh, C.A., Miller, J.E. and Brooks, C.E. (1992) Producing and Avoiding Stress Shielding. *Clinical Orthopaedics and Related Research*, **274**, 79-96. https://doi.org/10.1097/00003086-199201000-00010

[11] Rose, F.R.A.J. and Oreffo, R.O.C. (2002) Bone Tissue Engineering: Hope vs Hype. *Biochemical and Biophysical Research Communications*, **292**, 1-7. https://doi.org/10.1006/bbrc.2002.6519

[12] Swetha, M., Sahithi, K., Moorthi, A., Srinivasan, N., Ramasamy, K. and Selvamurugan, N. (2010) Biocomposites Containing Natural Polymers and Hydroxyapatite for Bone Tissue Engineering. *International Journal of Biological Macromolecules*, **47**, 1-4. https://doi.org/10.1016/j.ijbiomac.2010.03.015

[13] Barone, D.T., Raquez, J. and Dubois, P. (2011) Bone-Guided Regeneration: From Inert Biomaterials to Bioactive Polymer (Nano)composites. *Polymers for Advanced Technologies*, **22**, 463-475. https://doi.org/10.1002/pat.1845

[14] Sun, F., Zhou, H. and Lee, J. (2011) Various Preparation Methods of Highly Porous Hydroxyapatite/Polymer Nanoscale Biocomposites for Bone Regeneration. *Acta Biomaterialia*, **7**, 3813-3828. https://doi.org/10.1016/j.actbio.2011.07.002

[15] Rogel, M.R., Qiu, H. and Ameer, G.A. (2008) The Role of Nanocomposites in Bone Regeneration. *Journal of Materials Chemistry*, **18**, 4233-4241. https://doi.org/10.1039/b804692a

[16] Rajkumar, M., Meenakshisundaram, N. and Rajendran, V. (2011) Development of Nanocomposites Based on Hydroxyapatite/Sodium Alginate: Synthesis and Characterisation. *Materials Characterization*, **62**, 469-479. https://doi.org/10.1016/j.matchar.2011.02.008

[17] Noor, Z. (2013) Nanohydroxyapatite Application to Osteoporosis Management. *Journal of Osteoporosis*, **2013**, Article ID: 679025. https://doi.org/10.1155/2013/679025

[18] Wang, L., Li, Y. and Li, C. (2008) *In Situ* Processing and Properties of Nanostructured Hydroxyapatite/Alginate Composite. *Journal of Nanoparticle Research*, **11**, 691-699. https://doi.org/10.1007/s11051-008-9431-y

[19] Murugan, R. and Ramakrishna, S. (2004) Bioresorbable Composite Bone Paste Using

Polysaccharide Based Nano Hydroxyapatite. *Biomaterials*, **25**, 3829-3835. https://doi.org/10.1016/j.biomaterials.2003.10.016

[20] Yamaguchi, I., Tokuchi, K., Fukuzaki, H., Koyama, Y., Takakuda, K., Monma, H., *et al*. (2001) Preparation and Microstructure Analysis of Chitosan/Hydroxyapatite Nanocomposites. *Journal of Biomedical Materials Research*, **55**, 20-27. https://doi.org/10.1002/1097-4636(200104)55:1<20::aid-jbm30>3.3.co;2-6

[21] Lin, H. and Yeh, Y. (2004) Porous Alginate/Hydroxyapatite Composite Scaffolds for Bone Tissue Engineering: Preparation, Characterization, and *in Vitro* Studies. *Journal of Biomedical Materials Research Part B*: *Applied Biomaterials*, **71**, 52-65. https://doi.org/10.1002/jbm.b.30065

[22] Maruyama, M., Terayama, K., Ito, M., Takei, T. and Kitagawa, E. (1995) Hydroxyapatite Clay for Gap Filling and Adequate Bone Ingrowth. *Journal of Biomedical Materials Research*, **29**, 329-336. https://doi.org/10.1002/jbm.820290308

[23] Ribeiro, C.C., Barrias, C.C. and Barbosa, M.A. (2004) Calcium Phosphate-Alginate Microspheres as Enzyme Delivery Matrices. *Biomaterials*, **25**, 4363-4373. https://doi.org/10.1016/j.biomaterials.2003.11.028

[24] Sivakumar, M. and Rao, K.P. (2003) Preparation, Characterization, and *in Vitro* Release of Gentamicin from Coralline Hydroxyapatite-Alginate Composite Microspheres. *Journal of Biomedical Materials Research Part A*, **65**, 222-228. https://doi.org/10.1002/jbm.a.10495

[25] Teng, S., Shi, J., Peng, B. and Chen, L. (2006) The Effect of Alginate Addition on the Structure and Morphology of Hydroxyapatite/Gelatin Nanocomposites. *Composites Science and Technology*, **66**, 1532-1538. https://doi.org/10.1016/j.compscitech.2005.11.021

[26] Qiu, M.D., Yan, W.X., Li, X., Mei, L.H. and Yao, Z.H. (2013) Preparation and Microanalysis of Hydroxyapatite/Chitosan-Sodium Alginate Composite Materials. *Materials Review*, **27**, 60-62.

[27] Tolba, E., *et al*. (2010) Biomimetic Synthesis of Guided-Tissue Regeneration Hydroxyapatite/Polyvinl Alcohol Nanocomposite Scaffolds: Influence of Alignate on Mechanical and Biological Properties. *Journal of American Science*, **6**, 239-249.

[28] Daemi, H. and Barikani, M. (2012) Synthesis and Characterization of Calcium Alginate Nanoparticles, Sodium Homopolymannuronate Salt and Its Calcium Nanoparticles. *Scientia Iranica*, **19**, 2023-2028. https://doi.org/10.1016/j.scient.2012.10.005

[29] Berzina-Cimdina, L. and Borodajenko, N. (2012) Research of Calcium Phosphates Using Fourier Transform Infrared Spectroscopy. In: Theophanides, T., Ed., *Infrared Spectroscopy—Materials Science*, *Engineering and Technology*, InTech, 125-141. https://doi.org/10.5772/36942

[30] Liao, C., Lin, F., Chen, K. and Sun, J. (1999) Thermal Decomposition and Reconstitution of Hydroxyapatite in Air Atmosphere. *Biomaterials*, **20**, 1807-1813. https://doi.org/10.1016/s0142-9612(99)00076-9

[31] Venkatasubbu, G.D., Ramasamy, S., Ramakrishnan, V. and Kumar, J. (2011) Hydroxyapatite-Alginate Nanocomposite as Drug Delivery Matrix for Sustained Release of Ciprofloxacin. *Journal of Biomedical Nanotechnology*, **7**, 759-767. https://doi.org/10.1166/jbn.2011.1350